Interzone Microtubule Behavior in Late Anaphase and Telophase Spindles

William M. Saxton and J. Richard McIntosh

Department of Molecular, Cellular, and Developmental Biology, University of Colorado, Boulder, Colorado 80309

Abstract. We have studied microtubule behavior in late anaphase and telophase spindles of PtK_1 cells, using fluoresceinated tubulin (DTAF-tubulin), microinjection, and laser microbeam photobleaching. We present the results of two novel tests which add to the evidence that DTAF-tubulin closely mimics the behavior of native tubulin in vivo. (*a*) Microinjected DTAF-tubulin was as effective as injected native tubulin in promoting division of taxol-dependent mitotic mutant cells that had been deprived of taxol. (*b*) Microinjected colchicine-DTAF-tubulin complex was similar to injected colchicine–native tubulin complex in causing depolymerization of spindles.

Immediately after microinjection of DTAF-tubulin into wild-type cells during late anaphase or telophase, fluorescence incorporation by microtubules was seen in chromosomal half-spindles and just behind the chromosomes, but there was no fluorescence incorporation near the middle of the interzone. Over the next few minutes, tubulin fluorescence accumulated at the center of the interzone (the equator), becoming progressively more intense. In other experiments, cells were microinjected with DTAF-tubulin at prophase and allowed to equilibrate for 30 min. Cells that had progressed to late anaphase were then photobleached to reduce the fluorescence in the central portion of the interzone. Over a period of several minutes, the only substantial redistribution of fluorescence was the appearance of a bright area at the equator of the interzone. Both the site of fluorescence incorporation and the photobleaching data suggest that tubulin adds to the elongating spindle interzone near the equator where the plus ends of the interdigitated microtubules are located.

In further experiments, several dark lines were photobleached perpendicular to the pole-to-pole axis of fluorescent anaphase–telophase spindles. Time-dependent changes in the spacings between the lines indicated that the two halves of the interzone lying on opposite sides of the spindle equator moved away from one another. This shows that the interdigitated microtubules, which make up most of the interzone, can undergo antiparallel sliding. Our data support a model for anaphase B in which plus end elongation of interdigitated microtubules and antiparallel sliding contribute to chromosome separation.

THE mitotic spindles of many cells elongate during late anaphase and telophase, increasing the separation between the already segregated sets of chromosomes. A lengthening of the microtubules that connect the spindle poles is usually associated with this process (30, 42, 43). Although there do not appear to be single microtubules that run from one spindle pole to the other during anaphase, microtubules do provide a structural, interpolar link. The link is constructed from two sets of microtubules whose minus ends reside at the poles and whose plus ends extend past the equator into the opposite half-spindle (9, 30, 43). Due to the overlapping of these two sets at the spindle equator, they are known as "interdigitated microtubules." Fine-structure studies indicate that in the zone of overlap neighboring microtubules of opposite polarity interact with one another (26, 44). Because this pole-to-pole link elongates as the spindle poles move apart, the behavior of interdigitated microtubules must be a part of spindle elongation and the associated chromosome movement.

Several models for the participation of microtubules in spindle elongation have been proposed. An important early suggestion was that subunits add to microtubules all along their walls. The forced extension of microtubule lengths in the interzone would then push the spindle poles apart (17, 33). The more recent hypothesis that polymerization is an end-dependent process has led to proposals that subunits add to the minus ends of the interdigitated microtubules. Again, the extension of microtubule lengths would force the spindle poles apart (3, 22, 34). The alternative proposal is that subunits add to the plus ends of the interdigitated microtubules. Since this might be expected simply to extend the plus ends farther into the opposite half-spindles, the proposal also calls for the generation of a force that slides the two sets of interdigitated microtubules apart ("antiparallel sliding") as subunit addition proceeds (24, 29). Some workers have proposed that such a force could be generated by a cross-bridge cycle operating between the interdigitated microtubules from opposite half-spindles (24, 29, 42), but others have suggested

that there is a force generated outside the spindle that pulls the half-spindles apart (1, 15, 19). Although other variations have been proposed, these models are sufficient to focus attention on three important questions. (*a*) Where do subunits add to the interdigitated microtubules? (*b*) Do the interdigitated microtubules slide apart? (*c*) Where is the force generated that moves the spindle poles apart?

Data that address these questions are absent or conflicting. The site of subunit addition to interdigitated microtubules has not been identified for any organism in vivo. There are indications that interphase and some mitotic microtubules preferentially add tubulin to their plus ends (32, 38, 39), and recent work shows that addition to the plus ends of interdigitated microtubules can occur in vitro (25). Antiparallel sliding can occur in the highly organized central spindles of some diatoms (7, 20), but there is evidence that sliding does not occur in some other spindles (43). Some observations place the site of force generation for spindle elongation within the spindle (2, 7, 8, 20), while others place it outside the spindle (1, 19). Part of this confusion is probably due to the wide variety of organisms upon which these observations have been made, and part may be due to the sometimes indirect relationship between the observations made and the conclusions drawn.

The experiments described in this paper were aimed at studying spindle elongation in the mammalian cell line PtK_1. They have yielded data that address the three questions described above, all within the same cell type. Using techniques of fluorescence analogue cytochemistry and fluorescence redistribution after photobleaching (FRAP)[1] we have found evidence suggesting that (*a*) tubulin adds to the plus ends of interdigitated microtubules and not to their walls during late anaphase-telophase; (*b*) antiparallel sliding of the interdigitated microtubules can occur in vivo; and (*c*) a force for sliding may be generated in the interzone of the spindle. The significance of these results is discussed with respect to spindle elongation and microtubule dynamics in general.

Materials and Methods

Tubulin Preparation and Fluoresceination

Microtubules were prepared from clarified bovine brain homogenate by two cycles of temperature-dependent assembly-disassembly as described by Weingarten et al. (46). Polymerized tubulin was fluoresceinated using the method of Keith et al. (18) as modified by Leslie et al. (21). Assembled microtubules were suspended at ~10 mg/ml by gentle homogenization in a labeling buffer consisting of 100 mM 2[*N*-morpholino]ethanesulfonic acid (MES) at pH 7.5, 4 M glycerol, 1 mM EGTA, 1 mM $MgSO_4$, and 0.1 mM GTP. The pH was then adjusted to a final value of 7.0 by addition of either KOH or HCl. After 10 min at 37°C, a 50-fold molar excess of dichlorotriazinyl-aminofluorescein (DTAF) in .05 vol DMSO was rapidly mixed in. The reaction mixture was incubated for 10 min at 37°C and then centrifuged at 125,000 *g* for 30 min at 37°C.

The pellet from the reaction mixture contained fluorescent microtubules, aggregated proteins, and a substantial amount of free DTAF. Active fluorescent tubulin (DTAF-tubulin) was purified from the labeling mixture by cycles of assembly and disassembly. The first pellet was resuspended by homogenization at ~10 mg/ml in a tubulin polymerization buffer developed by Hamel and Lin (14) (1 M Na-glutamate, 1 mM EGTA, and 0.1 mM GTP at pH 6.9 [GEG]). The suspension was placed in an ice bath for 20–30 min to promote depolymerization, then centrifuged at 125,000 *g* at 4°C for 30 min. The supernatant was collected, brought to 0.3 mM GTP, and placed in a 37°C shaker bath for 20 min to promote polymerization. Microtubules were pelleted, and the supernatant was discarded. This procedure of depolymerization-repolymerization in GEG was repeated for a total of 4.5 cycles. The protein concentration in resuspension steps was maintained between 2 and 4 mg/ml until the final one. The final DTAF-tubulin solution was frozen in liquid nitrogen at ~10 mg/ml in 10- or 100-μl aliquots.

DTAF-tubulin prepared in this manner appeared to be free of microtubule-associated proteins and unbound dye. The molar ratio of fluorescein/tubulin-dimer was approximately 1 (21). Final yield of polymerization-competent tubulin varied from one preparation to another between 3 and 10% of the total protein present in the initial reaction mixture.

Native tubulin (unlabeled) was prepared for use in control experiments by using the DTAF–tubulin labeling and purification procedure with the omission of the DTAF reaction step.

Preparation of Colchicine-complexed Tubulin

Colchicine–tubulin complexes were produced by incubating either native or DTAF-tubulin at 100 μM with 500 μM colchicine for 2 h at 37°C in GEG. After passage through a Biogel P10 filtration column to remove unbound colchicine, the colchicine/tubulin-dimer ratios were ~1:1. The colchicine–tubulin complexes were stabilized until injection (<1 h) by storage at 4°C. The half-time for dissociation of the complex is ~48 h at 37°C ($k_d = 4.2 \times 10^{-6}$/s) (10) and significantly slower at 4°C.

Cell Culture

PtK_1 cells were grown in a 5% CO_2 incubator at 37°C in Ham's F-12K supplemented with 10% FBS. Cells were plated on 22- × 22-mm coverslips for experiments and were usually used when the cells were 80–95% confluent. During microinjection, the cells were transferred to Ham's F-12, 10% FBS, and 20 mM Hepes buffer. The mutant Chinese hamster ovary (CHO) cell line Tax-18 was cultured as described by Cabral and Gottesman (5) with the addition of 0.2 μg/ml taxol to the culture medium.

Microinjection and Observation

Protein solutions were prepared for microinjection by dialysis against 10,000 vol of an injection buffer consisting of 100 mM glutamic acid, 140 mM KOH, 20 mM citric acid, 1 mM $MgSO_4$, 1 mM EGTA, and 0.1 mM GTP at pH 7.0. This buffer was chosen because it served to stabilize the polymerization competence of tubulin and was not visibly deleterious to cells when microinjected. The pipette microinjection technique of Graessmann et al. (12), as modified by Zavortink et al. (47), was normally used to deliver an amount of protein solution equal to ~10% of a cell's volume. Tubulin concentrations of 20–60 μM were injected unless otherwise noted. Assuming that the endogenous tubulin concentration is ~20 μM (16), the molar ratio of injected to endogenous tubulin varied from 1:10 to 1:3.

All microinjections were performed on a Zeiss Universal microscope equipped with a 40×, phase-contrast, water immersion lens (NA 0.75). In studies of DTAF–tubulin incorporation by mitotic microtubules, PtK_1 cells were microinjected at 36 ± 1°C in an open chamber in which the cells' environment was controlled by perfusion with 36°C medium. The temperature of the medium was monitored within 2 mm of the cells under study. Observation by epifluorescence was begun within 5 s of microinjection. For studies of FRAP, cells were injected at room temperature, and returned to a CO_2 incubator at 37°C for 30 min to allow recovery and equilibration. Coverslips were then mounted in culture medium on slides, using strips of parafilm for spacers and a mixture of paraffin, vaseline, and lanolin (1:1:1) as a sealant. Observations were made with a 63× planapochromat oil immersion lens (NA 1.4) and epifluorescence illumination. Temperature was maintained at 36 ± 1°C during observation with a model 279 Sage air curtain incubator and a Yellow Springs electric thermometer with a microthermistor placed in the immersion oil of the objective lens.

Microinjections of colchicine-tubulin into metaphase PtK_1 cells were done at 36 ± 1°C in the open perfusion chamber. Polarization optical images of spindle birefringence were obtained with a strain-free condenser, the 40× water immersion lens (especially selected for reduced strain), crossed polaroid filters, and a lambda/30 Brace-Koehler rotary compensator. A spindle was oriented so that its pole-to-pole axis was at 45° with respect to the plane of polarization and the compensator was adjusted for maximum image contrast on a video monitor. A polarization optical image was recorded, the optics were switched to phase contrast, the cell was injected, and then the optics were quickly (5 s) switched back to the polarization configuration to record the effects of microinjection.

To visualize fluorescence in microinjected cells with a minimum of the

1. *Abbreviations used in this paper*: DTAF, dichlorotriazinyl-aminofluorescein; FRAP, fluorescence redistribution after photobleaching.

unwanted general photobleaching that occurs during epifluorescence observation, we used a low light level video microscopy system with a specimen shielding shutter in the illumination path. A Dage ISIT video camera mounted on a Zeiss Universal microscope was coupled to an IRIS computer (Silicone Graphics Inc., Mountain View, CA) equipped with a video image processing system made by G. W. Hannaway and Associates (Boulder, CO). Images were viewed on and photographed from a Zenith television monitor. To improve the signal-to-noise ratio in the intensified video signal, the computer averaged 128 video frames (4 s) for each image and stored the average in a frame buffer. The image was then read to a digital disc, and later processed to correct for the systematic intensity distortions produced by the video camera (Stemple, D. L., S. Sweet, M. J. Welsh, and J. R. McIntosh, manuscript in preparation). 35-mm film micrographs, made directly from the microscope, had better spatial resolution than the video micrographs, but only one image could be obtained before the specimen was completely photobleached. With the intensified video camera, one sacrifices spatial resolution for the ability to take up to 20 micrographs of the same cell. To follow a fluorescent cell over extended periods, the duration of epifluorescence illumination was limited to the time intervals necessary for each image. The IRIS was programmed to open the specimen shielding shutter on command or at pre-set times. The computer then waited for 1/15 s to allow the video signal to stabilize, and began to average and store the image. When averaging was complete, the specimen shielding shutter closed.

FRAP Technique

FRAP experiments involved an integrated use of the video microscope system and a laser microbeam photobleaching apparatus. The light beam for photobleaching was generated by a 2-W argon ion laser (Spectra-Physics, Inc., Mountain View, CA) tuned to the 488-nm line. The 1-mm diameter beam was directed into the epifluorescence tube of the microscope where it was reflected by a cubic beamsplitter to become coaxial with the illumination path. After traveling forward to the dichroic mirror and then reflecting downward, the beam was demagnified by the objective lens (63×) to a diameter of ~40 μm at the specimen plane. The beam geometry was controlled by placing masks in the beam path at a plane conjugate to the specimen. Slot bleaches were performed using a beam aperture 200 μm wide and 2 mm long. The slot-shaped cross section of the microbeam at the specimen was ~7 × 40 μm. Grating bleaches were performed using a Ronchi grating of 119 lines/cm. The Ronchi grating produced a periodic pattern of bright and dark lines at the specimen (period of 2.9 μm). Microbeam pulse durations varied from 50–200 ms, depending on the fluorescence intensity of the specimen.

In a typical experiment, a prebleach image of a fluorescent cell was averaged and recorded, then the cell was irradiated with the microbeam. The duration of the laser pulse was controlled with a shutter in the beam path driven by a timer circuit designed and built by E. D. Salmon (University of North Carolina). The firing of the laser microbeam triggered a series of postbleach images at programmed time intervals after the pulse.

Data Analysis

For analysis of the effects of colchicine injections on spindle birefringence, measurements of light intensity in specified regions of stored video images were made using the IRIS computer and software developed by Derek Stemple (G. W. Hannaway and Associates, Boulder, CO) which will be described elsewhere (Stemple, D. L., S. Sweet, M. J. Welsh, and J. R. McIntosh, manuscript in preparation). Briefly, a line was drawn with a video cursor around a portion of an image of a cell (e.g., a birefringent spindle). The computer then determined the average light intensity per video pixel within the boundary. The same boundary line was used to measure intensity values of the same portion of the cell in images at subsequent time points in a particular series. Points describing the average intensity as a function of time were fitted with a quartic polynomial to model changes in spindle birefringence.

Fluorescence videomicrographs of grating photobleaches were analyzed for relative spindle interzone movements using the IRIS computer. Software was designed to mimic the action of a scanning microdensitometer. A boundary was drawn with the video cursor to surround the portion of the image to be analyzed. The average pixel intensity for each vertical column of pixels within the boundary was calculated, and recorded as a function of horizontal position. A plot of intensity vs. position was automatically displayed. Positions of intensity maxima and minima were marked on the plot by eye using the cursor to identify the relevant pixels. Two values for each point were averaged and recorded. This process was repeated for each image in a FRAP series, yielding a data set that could be analyzed to determine the changes as a function of time in the horizontal position of the pixels corresponding to intensity maxima and minima (1 pixel = 0.18 μm).

Immunofluorescence

For immunofluorescence staining, PtK_1 cells grown on coverslips were lysed for 30 s in 0.1 M Pipes, 1 mM $MgSO_4$, 1 mM EGTA, 0.5% Triton X-100, pH 6.9, at 37°C. Coverslips were transferred to fixative (0.1% glutaraldehyde, 2% paraformaldehyde, 0.1 M Pipes, 1 mM $MgSO_4$, and 1 mM EGTA, pH 6.9) at 37°C for 15 min. They were rinsed in PBS, transferred to a 0.5% solution of Na-borohydride in PBS, and then rinsed three times for 5 min each time in PBS. Coverslips were incubated with a 1:50 dilution of monoclonal anti-tubulin antibody for 1 h at 37°C, rinsed three times for 5 min each time in PBS, incubated with a 1:100 dilution of fluorescein-conjugated rabbit anti-mouse antiserum for 1 h at 37°C, rinsed three times for 5 min each time in PBS, and mounted on slides with 90% glycerol, 0.1% $NaHCO_3$, 2% *N*-propyl gallate, at pH 8.2. Fluorescence micrographs were taken using a Zeiss 63× planapochromat lens and Kodak technical pan film developed for reduced contrast in HC110 dilution F.

Results

In Vivo Comparison of Native and DTAF-Tubulin

The interpretation of results obtained using derivatized tubulin depends on an understanding of its behavior in living cells. We have compared the behavior of native and DTAF-tubulin in vivo by determining their relative abilities to rescue taxol-dependent tissue culture cells grown under nonpermissive culture conditions. Tax-18 cells (kindly provided by F. R. Cabral and M. J. Schibler) (4, 6) were plated on coverslips and incubated for 24 h in permissive medium (with taxol), then transferred to nonpermissive medium (without taxol) for 4–8 h. Solutions of either fluorescent ovalbumin, fluorescent tubulin, or native tubulin plus fluorescent ovalbumin were prepared and the total protein concentration of each solution was brought to 11 mg/ml by addition of native ovalbumin. The solutions were coded to avoid bias during microinjection and scoring. Cells were injected with 10–30% cell volumes of the solutions and returned to an incubator in nonpermissive medium for 12–20 h. They were then mounted for epifluorescence observation and scored as divided (pairs of adjacent, fluorescent cells) or undivided (single fluorescent cells). Results of these experiments are presented in Table I. Roughly 20% of the cells were able to complete a division after an injection of ovalbumin alone. This value held regardless of the concentration of ovalbumin injected and was judged to be the background level of division under the conditions used. The background was not unexpected, since the Tax-18 clone used is not a severe mitotic mutant (6). Microinjections of both DTAF-tubulin and native tubulin at 8 mg/ml increased the percentage of successful divisions. Native tubulin appeared to be slightly more effective than DTAF-tubulin in effecting rescue.

In a second set of control experiments we took advantage of the slow dissociation of colchicine from tubulin to compare further the behaviors of native and DTAF-tubulin in vivo. The effects of microinjecting either colchicine-tubulin, colchicine-DTAF-tubulin, or free colchicine plus BSA on the birefringence and the function of PtK_1 spindles were examined. Either colchicine-tubulin or colchicine-DTAF-tubulin solutions at 10 μM (injection ≤10% cell volume) caused a rapid loss of spindle birefringence and prevented anaphase. The extent of birefringence loss was 59 ± 16% (n = 11) for colchicine-tubulin injections and 42 ± 13% (n = 12) for

Table I. Recovery of Mitotic Ability Following Protein Injection

Protein injected	Concentration	Single cells	Cell pairs	Percent divided
	mg/ml	*n*	*n*	
Ovalbumin	2–3	268	54	17
	8–11	301	79	21
Native tubulin	0.5	55	18	25
	2	48	25	25
	5	11	7	39
	8	179	185	51
DTAF-tubulin	0.5	30	6	17
	2	38	7	16
	5	28	22	44
	8	120	81	40

colchicine-DTAF-tubulin injections. Colchicine albumin injections (10 μM free colchicine) resulted in a smaller loss of spindle birefringence (25 ± 11%), and was often followed by a normal anaphase (data reported in preliminary form in reference 31). This study indicates that DTAF-tubulin can participate normally in the pathway of colchicine-induced spindle depolymerization, although it may be slightly less effective than native tubulin.

Microtubules in Late Anaphase and Telophase Seen with DTAF-Tubulin and with Anti-Tubulin Immunofluorescence

DTAF-tubulin was used to study the distribution of microtubules during late anaphase and telophase in living PtK_1 cells. Previous experiments (37) and those described above suggest that microtubules incorporate DTAF-tubulin and fluoresce brightly. Cells were microinjected at prophase, allowed to equilibrate for 30 min, and observed as they proceeded through anaphase and telophase. Typical patterns of the fluorescence seen are shown in Fig. 1. The separated groups of chromosomes are visible as dark regions (Fig. 1 *A*, *arrowheads*). Coarse, well-defined fibers are seen between the two groups of chromosomes (the interzone) near the equator. A bright but more diffuse fluorescence is seen in the regions of the interzone adjacent to the chromosomes and around the poles. As anaphase proceeded into telophase, the fibers retained their fluorescence throughout the interzone as they were bundled together by the cleavage furrow.

In most aspects the DTAF–tubulin fluorescence patterns shown in Fig. 1 correlate well with spindle microtubule patterns seen using higher resolution methods such as immunofluorescence. Using anti–tubulin antibody to probe PtK_1 cells fixed at various stages of anaphase and telophase, it was seen that the coarse fibers correspond with bundles of interzone microtubules (Fig. 2). Fine structure work has shown that most of these are interdigitated microtubules (27, 28). While the fluorescence of DTAF-tubulin is continuous through the equator, the anti–tubulin staining is not. The dark zone seen at the equator in Fig. 2 *C* is probably an artifact of immunostaining. Antibodies often do not bind to microtubules in that zone, perhaps because of the presence of a dense proteinaceous matrix ("midbody material"; see references 27, 28). The diffuse DTAF–tubulin fluorescence seen in the interzone near the chromosomes probably corresponds with the presence of polar as well as interdigitated microtubules. Some polar microtubules are visible in this region by immunofluorescence because of the high signal-to-noise ratio of this method. The DTAF–tubulin fluorescence near the poles probably represents the presence of several types of spindle microtubules, including polar, interdigitated, kinetochore, and astral fibers. This situation simplifies in telophase when the centrosomes begin to renucleate cytoplasmic microtubules (27).

Note that the dark regions that identify the chromosomes

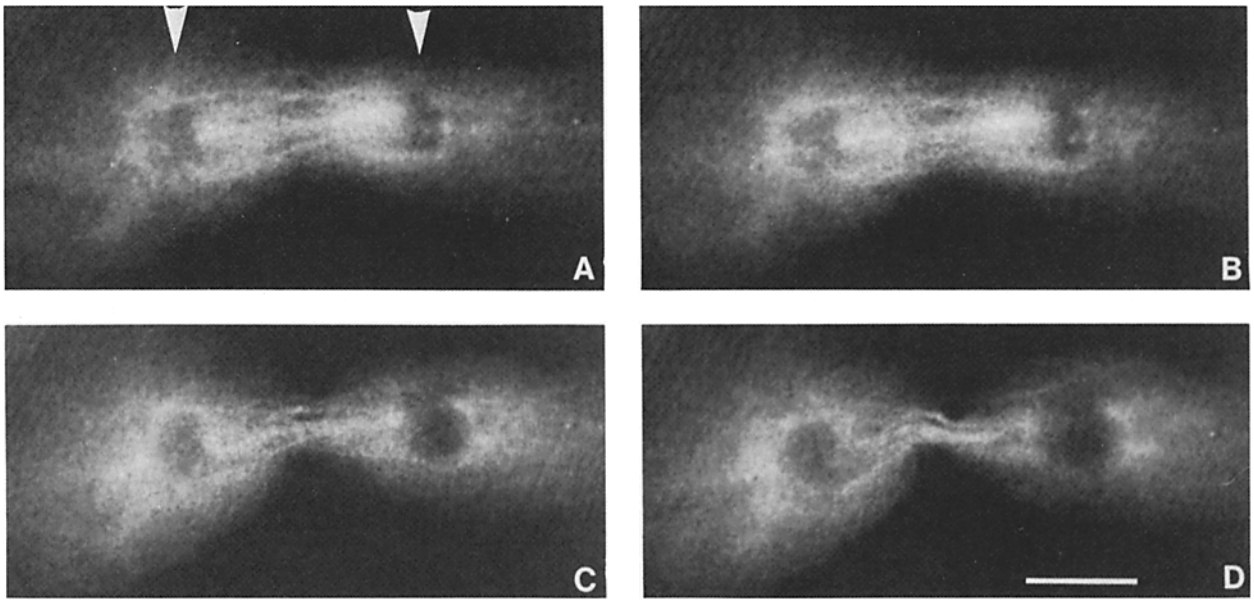

Figure 1. An example of the patterns of fluorescence seen during late anaphase-telophase in cells that were microinjected with DTAF-tubulin during prophase. Elapsed time after the first image was 60 (*B*), 420 (*C*), and 540 (*D*) s. Note that a fairly homogeneous fluorescence is maintained between the two groups of chromosomes (*arrowheads*) along the pole to pole axis. Bar, 10 μm.

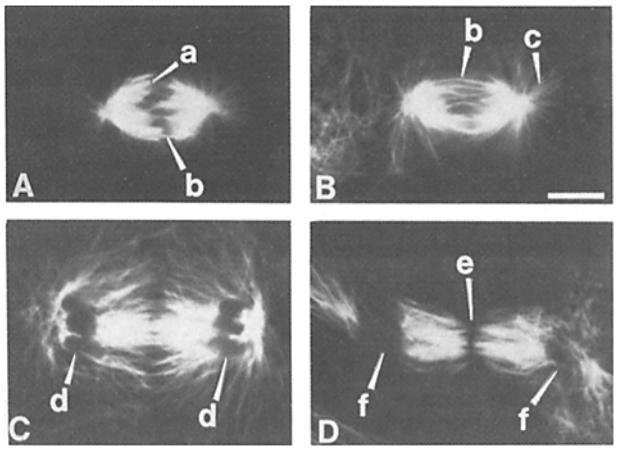

Figure 2. Anti-tubulin immunofluorescence images of anaphase and telophase PtK_1 cells. *A* shows a spindle in early anaphase. The kinetochore fibers (*a*) had shortened slightly as the chromosomes moved toward the poles. Note the presence of a few interzone fibers (*b*). *B* shows a spindle in midanaphase. Note the prominent interzone fibers (*b*) and the astral fibers (*c*). *C* shows a late anaphase spindle with a well-developed interzone. Note the chromosome-shaped dark areas near the poles (*d*). It appears that some of the interzone microtubules no longer extend to the poles. Alternatively, antibody-binding sites may be masked, or the chromatin may become opaque to fluorescence at this stage. *D* shows a telophase spindle. The dark zone at the equator (*e*) is due to a masking of the microtubules there, perhaps by midbody material. Note that the interzone microtubules appear to end at the inner sides of the reforming nuclei (*f*). The poles on the outer sides had begun renucleating interphase cytoplasmic microtubules. Bar, 10 μm.

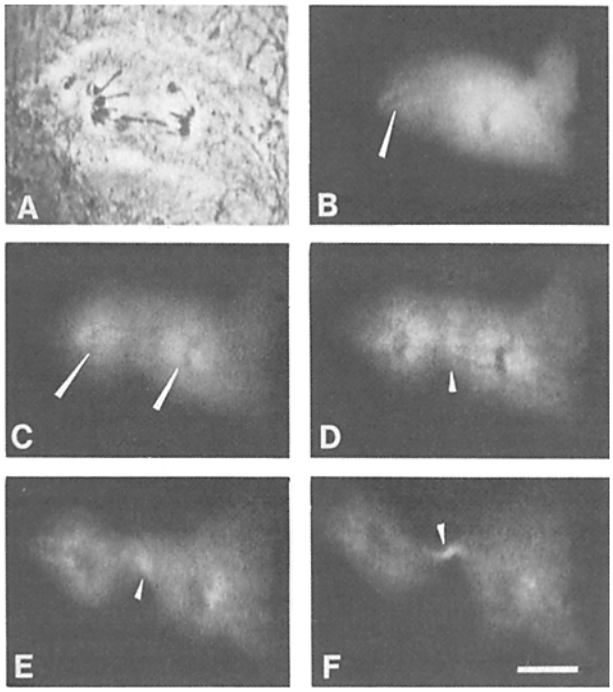

Figure 3. Patterns of incorporation of DTAF-tubulin by anaphase–telophase spindles. Late-anaphase cells, maintained on the microscope stage under physiological conditions, were microinjected with DTAF-tubulin. *A* is a phase-contrast video micrograph of a cell before microinjection. The subsequent video micrographs show the patterns of fluorescence that developed after microinjection. The times elapsed after injection were 5 (*B*), 65 (*C*), 305 (*D*), 545 (*E*), and 845 (*F*) s. The injection site was near the right margin of the cell. Note that as the soluble DTAF-tubulin diffused across the cell, there was a rapid incorporation of fluorescence above background by the chromosomal half-spindles (*long arrowheads*, *B* and *C*). This was followed by a slower fluorescence incorporation at the equator of the interzone (*short arrowheads*, *D*–*F*). Note that there were areas of the interzone on either side of the equator that remained dim. Bar, 10 μm.

are present in the DTAF–tubulin images as well as the immunofluorescence images late in anaphase. Either microtubules were absent there or the chromatin blocked the fluorescence. If the latter is true, it is a property achieved only in late anaphase because during earlier stages of mitosis such a blockage of DTAF–tubulin fluorescence has not been seen (31, 35, 37, 45). At the end of anaphase when the chromatin decondenses, the nuclear membrane reforms, and the centrosomes begin renucleating cytoplasmic microtubules, it appears that the interzone microtubules are separated from the poles (Fig. 1, *C* and *D*, and Fig. 2, *C* and *D*). It may be that the dark regions seen at late anaphase are due to the beginnings of this pole detachment process.

DTAF-Tubulin Incorporation into Anaphase-Telophase Spindles

Cells injected during late anaphase-telophase produced spindle fluorescence patterns different from those seen in late anaphase–telophase cells that had been injected during prophase, as described above. Late anaphase PtK_1 cells, maintained under physiological conditions, were injected with DTAF-tubulin and immediately observed with epifluorescence illumination. Fig. 3 shows that fluorescence incorporation was heterogeneous along the spindle axis. As the labeled tubulin diffused across the cell, it was rapidly taken up by the chromosomal half-spindles (the area between a pole and its chromosomes). The nonspecific distribution of fluorescence in images of anaphase cells microinjected with rhodamine-labeled actin argues that this elevated chromosomal half-spindle fluorescence seen with DTAF-tubulin is due to a specific incorporation of this protein into spindle microtubules (37). Fluorescence in the interzone between the chromosomal half-spindles was limited at first to the background level produced by soluble DTAF-tubulin. Later, fluorescence above background appeared at the spindle equator, while the areas of the interzone between the chromosomal half-spindles and the equator remained dim. This heterogeneous pattern of DTAF–tubulin incorporation was unexpected, since earlier studies of incorporation in metaphase cells showed homogeneous fluorescence recruitment throughout the spindle (35, 37, 45). Cells injected during early anaphase also show homogeneous fluorescent tubulin incorporation (data not shown). It is evident that between early and late anaphase, microtubule behavior changes such that some areas of the spindle do not incorporate the microinjected tubulin, while others do. The pattern of incorporation and nonincorporation in the interzone that is seen in Fig. 3 does not reflect the presence and absence of spindle microtubules. Figs. 1 and 2 and many other studies (reviewed in reference 27) show that microtubules are present in the interzone throughout anaphase and telophase. Therefore, the patterns seen in Fig. 3 suggest that interzone microtubules

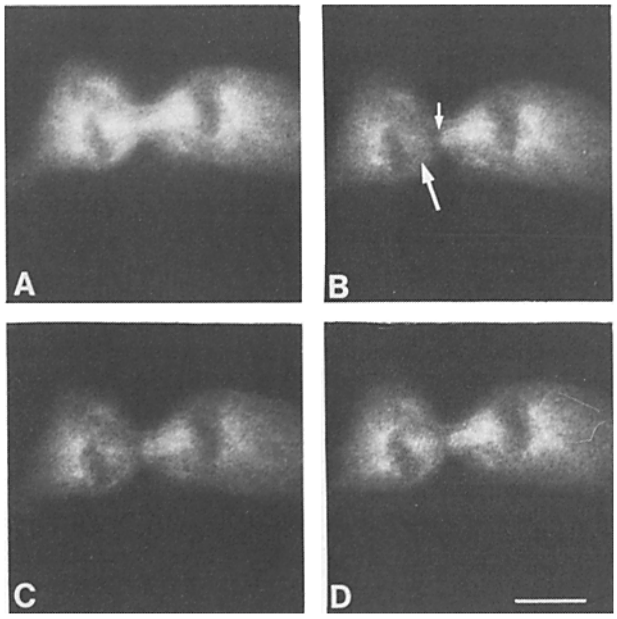

Figure 4. Relative microtubule turnover rates in chromosomal half-spindles and the adjacent late anaphase interzones. Prophase cells were microinjected with DTAF-tubulin and allowed to equilibrate for 30–60 min as in Fig. 1. Cells that had proceeded to late anaphase were irradiated with a laser such that the fluorescence was photobleached in a 4-μm spot between the trailing edge of one group of chromosomes and the equator. The redistribution of unbleached DTAF-tubulin into the spot was recorded with fluorescence video micrographs. A cell is seen (*A*) just before, (*B*) 3 s after, (*C*) 11 s after, and (*D*) 44 s after photobleaching. Note that the bleached part of the chromosomal half-spindle (*large arrow*) had already regained some fluorescent tubulin at 3 s and continued to brighten while the adjacent part of the interzone (*small arrow*) remained relatively dark. This demonstrates the heterogeneous rates of microtubule turnover seen in late anaphase–telophase spindles. Bar, 10 μm.

have sites of tubulin addition near the equator and resist tubulin addition in the flanking areas.

FRAP of Anaphase–Telophase Spindles

Because of our suspicion that microinjection disturbs a cell, and consequently that injection incorporation results might not represent normal spindle behavior, the question of microtubule dynamics in late anaphase–telophase spindles was pursued by studying fluorescence redistribution after photobleaching (FRAP). It has previously been shown that photobleaching of DTAF-tubulin–containing microtubules in vivo does not disturb their distribution or behavior in any noticeable way (35, 37). Prophase PtK_1 cells were microinjected with DTAF-tubulin, allowed to equilibrate for 30–60 min, and prepared for FRAP as described in Materials and Methods. To examine the relative behaviors of a chromosomal half-spindle and the adjacent interzone, an image of a cell with a fluorescent anaphase–telophase spindle was collected; then the region between the trailing edge of a group of chromatids and the equator of the interzone was photobleached with a 4-μm-diam microbeam (Fig. 4). After a 3-s pause to allow the diffusional redistribution of soluble DTAF-tubulin, a series of postbleach images was collected. Fig. 4 *B* shows that some fluorescence redistribution occurred in the region of the interzone near the chromosomes within 3 s after photobleaching. That area rapidly achieved full redistribution (Fig. 3 *D*). The part of the interzone near the equator showed little or no redistribution during the period of observation (70 s). This corroborates the injection incorporation results described above that show a heterogeneity of microtubule dynamics as a function of position in late anaphase–telophase spindles.

FRAP was also used to examine the equator as a site of tubulin addition to interzone microtubules. Anaphase spindles with well-defined, fluorescent interzones were aligned for photobleaching with a slot-shaped laser microbeam such that a 7-μm-wide dark zone was created at the equator. Images were collected before photobleaching, immediately after photobleaching, and then at subsequent times to record fluorescence redistribution. Fig. 5 demonstrates the results of such an experiment. Fluorescence above background first reappeared in the bleached region as streaks running parallel to the spindle axis (Fig. 5 *C*). At later times, the brightest fluorescence was seen as a band at the spindle equator.

There is a correlation between these fluorescence patterns and the distribution of the plus ends of interdigitated microtubules, as seen in fine structure studies of PtK_1 and *Dictyostelium* (9, 30). The plus ends of interdigitated microtubules from one pole appear to be distributed throughout the opposite half-spindle with more near the equator and fewer near the opposite pole during metaphase and early anaphase. Later in anaphase the interdigitated microtubules are generally found collected into the interzone fibers with plus ends again more numerous near the equator and less numerous away from it. As cells approach telophase the lengths of the interdigitated microtubules in the interzone fibers become more uniform such that essentially all their plus ends are located near the equator.

Grating Photobleaches and Antiparallel Microtubule Sliding

One possible mechanism for the motion of the plus ends of the interdigitated microtubules to the equator during spindle elongation is antiparallel microtubule sliding. To examine this possibility, we studied FRAP with a complex photobleaching pattern. A Ronchi grating placed in the laser path generated a microbeam geometry that photobleached a set of periodic lines perpendicular to the spindle axis. The initial periodicity was 2.9 μm from each bleached line to its neighbor. Fig. 6 shows the results of a grating FRAP experiment spanning late anaphase and telophase. The distance between two dark lines on either side of the equator was measured from photographic prints to be 3 μm 60 s after photobleaching. The same interval measured at 660 s was 4 μm, showing a net change of 1 μm. During that time, the distance between two lines on the same side of the equator did not change measurably. This suggests that the two halves of the interzone were sliding away from one another.

Measurement of the grating bleach periodicities made by hand from prints were informative but insufficient for accurate quantification of the apparent movement. To make such measurements more accurately, we used digital video image processing. Figs. 7–9 show the results and analysis of a grating FRAP experiment on one cell as it went through late anaphase and telophase. Fig. 7 shows the image series

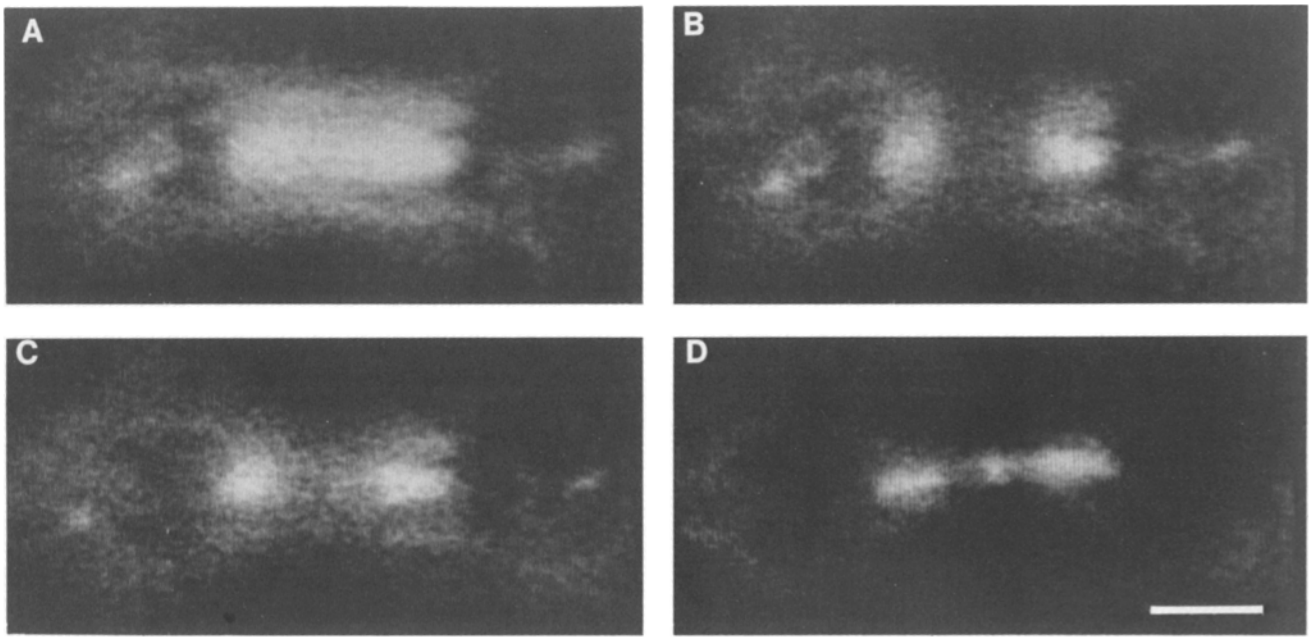

Figure 5. Patterns of fluorescence redistribution seen after a slot photobleach of the midregion of a late anaphase–telophase spindle. *A* shows the prebleach fluorescence pattern. Chromosomes had moved to the poles and the interzone microtubules were well organized. 1 s after laser irradiation (*B*) it was clear that the DTAF-tubulin in the equator region of the interzone had been bleached. 180 s after photobleaching (*C*), background fluorescence (soluble DTAF-tubulin) had redistributed into the bleached area, and fluorescence above background was seen in longitudinal streaks on either side of the equator. At 360 s (*D*) a bright, fluorescent region was seen at the equator flanked by two dark zones. These images suggest that tubulin adds to the elongating interdigitated microtubules near the equator of the interzone. Bar, 10 μm.

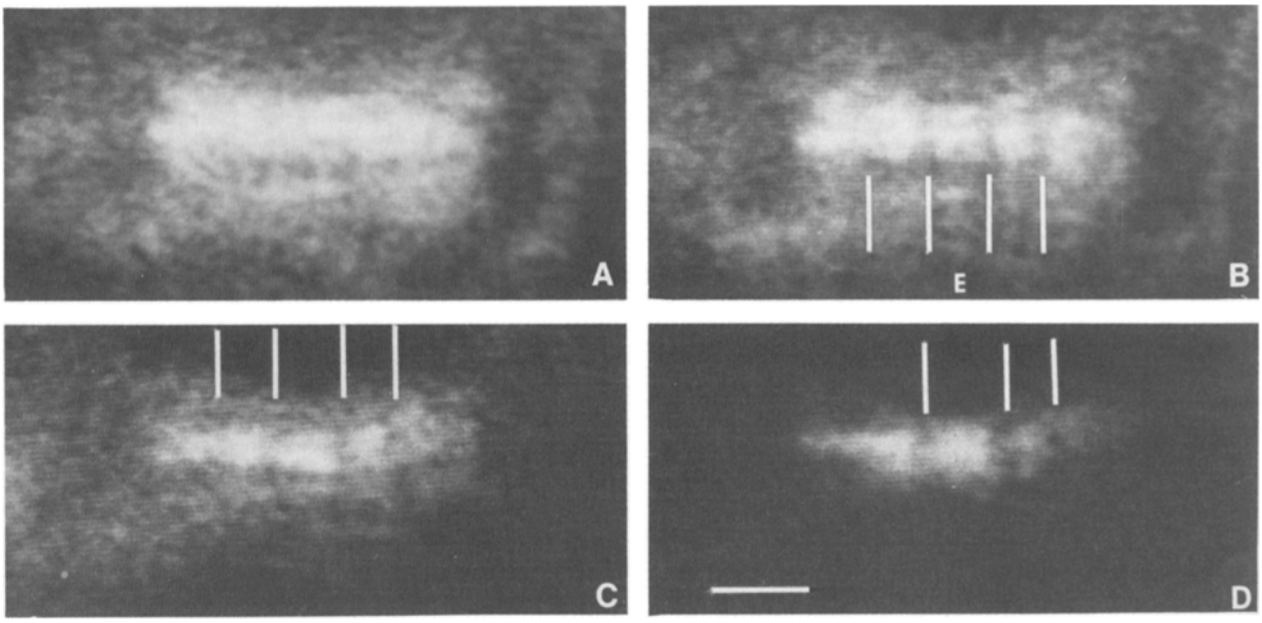

Figure 6. Fluorescence patterns seen in a late-anaphase–telophase cell after a grating photobleach. The fluorescence pattern of the cell immediately before bleaching is seen in *A*, then at 60 s (*B*), 420 s (*C*), and 660 s (*D*) after bleaching. The positions of bleach-induced fluorescence minima in the postbleach images were judged by eye and marked (*white lines*). Note the changes in spacing that occurred between the two fluorescence minima on either side of the equator (*E*) as telophase progressed. The distance between them increased from ~3 μm at 60 s (*B*) to ~4 μm at 660 s (*D*). The distance between dark lines that were on the same side of the equator did not increase appreciably during the period of observation. This suggests that the two half-spindles were sliding away from one another as units. The interzone fluorescence dominates the image at 660 s because its intensity increased relative to the rest of the cell as the cleavage furrow compacted it. Bar, 5 μm.

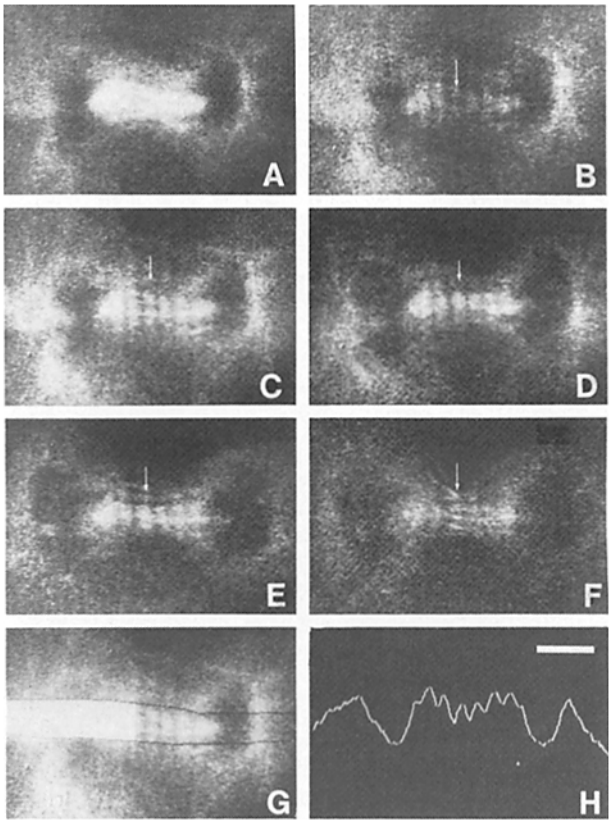

Figure 7. Another grating photobleach series and computer-aided analysis. The fluorescence pattern of the cell is seen (*A*) immediately before and (*B*) immediately after laser irradiation. Epiillumination intensity was increased between 0 and 60 s to enhance contrast in the subsequent images. The cell is seen (*C*) 60 s after, (*D*) 420 s after, (*E*) 880 s after, and (*F*) 1,000 s after photobleaching. The arrows mark the approximate location of the equator. Points of maximum and minimum fluorescence were determined by using the computer as a scanning intensitometer. The region of the image to be scanned was outlined using a video cursor. The computer then calculated the average intensity of each vertical column of pixels within the boundary, marking completed columns white as it progressed from left to right (*G*). Average intensity within the boundary as a function of horizontal position on the image was displayed on the video screen (*H*). The video cursor was used to mark the horizontal position of bleach-induced intensity maxima and minima on the graph, and the computer then calculated the distances between them. Bar, 10 μm.

and demonstrates the method used for determining the positions of fluorescence intensity maxima and minima along the spindle axis (see also Materials and Methods). The distances between all maxima and minima were measured for each image in a FRAP series. Changes in the measurements were determined by subtracting each time zero distance from the corresponding distance measured at a later time point. The results of such an analysis of spacing changes between 0 and 880 s are displayed in terms of video pixels in the matrix seen in Fig. 8.

The data in Fig. 8 are collected into three groups representing movements within the left half-spindle, within the right half-spindle, and between the two. Changes between points that lie on the left side of the spindle equator are enclosed in the triangle at the upper left of the matrix, while changes between points that lie on the right side of the spindle equator are enclosed in the triangle at the lower right. Changes between points that lie on opposite sides of the equator are enclosed in the rectangle at the upper right. Measurements involving the fluorescence maximum at position 5 were not included in any of the three groups because of its proximity to the spindle equator. Note that there was little or no movement within the left and right half-spindles while distances between the two increased. Mean values for the amount of change between adjacent fluorescence maxima and minima in terms of μm (0.18 μm/pixel) are 0.1 ± 0.03 μm (n = 3) for the left half-spindle and −0.04 ± 0.02 μm (n = 5) for the right half-spindle. The mean for changes between the two half-spindles, 1.2 ± 0.2 μm (n = 4), was calculated from the values of changes between pairs of fluorescence maxima or minima that were symmetrically located with respect to position 5 (the equator). Note that this last set of four values represents movements between increasingly distant parts of the interzone. The amount of change appears to be independent of the distance between measuring points. This argues against mechanisms of interzone elongation that depend on the insertion of subunits all along the walls of the microtubules. Essentially all of the increase in spacing occurs between points 4 and 6. The asymmetry between movements measured from the left half-spindle and those measured from the right half-spindle to position 5 probably reflects the fact that position 5 is not directly on the spindle equator.

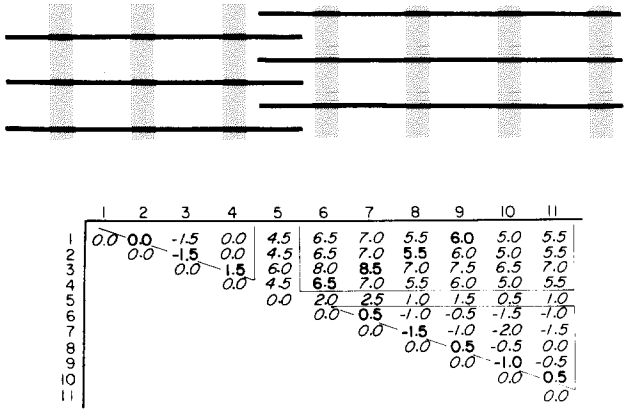

Figure 8. Changes in distances between the fluorescence maxima and minima in the cell shown in Fig. 7. A diagram of the bleached interzone is included above the matrix to demonstrate the relative positions of measuring points 1–11. Shaded bars represent fluorescence minima and intervening unshaded areas represent fluorescence maxima along the interzone. The matrix shows spacing changes between the maxima and minima from time 0 to 880 s (Fig. 7, *B* and *E*). Changes were calculated by subtracting from each measurement of the 880-s image the corresponding measurement of the time 0 image. Changes in distances between points that lie on the left side of the equator are enclosed in a triangle at the upper left of the matrix. Changes in distances between points that lie on the right side of the equator are enclosed in a triangle at the lower right of the matrix. Changes in distances between points that lie on opposite sides of the equator are enclosed in the rectangle at the upper right of the matrix. Note that points on opposite sides of the equator move away from one another while points on the same side do not. The mean spacing change for each of the three groups was calculated using the boldface values.

To determine rates of movement within the left half, within the right half, and between the two, the mean changes from each image in the FRAP series of Fig. 7 were plotted as a function of time (Fig. 9). Lines were fit to the data of each of the three sets of points by linear regression, forced through the origin. The slopes of the lines, measured in μm/s, were taken to represent average rates of motion. The use of straight lines to fit the data points is not meant to imply that the movement was linear with respect to time, but the straight line permits an estimate of the average rate of movement. Results from six different spindles are shown in Table II. The rates of movement between interzone halves in these experiments ranged from 0.04 to 0.18 μm/min. The variation may reflect the heterogeneity seen in the extent and rate of late anaphase and telophase spindle elongation in PtK_1 cells. The rates of movement within left and right halves of the interzone were near 0 or slightly negative.

Comparison of Movement Data with Images

The anti-tubulin immunofluorescence images in Fig. 2 suggest that most if not all microtubule connections between the spindle pole and interzone break in late anaphase-telophase during the period of observation in grating bleach experiments. In our fluorescence videomicrographs it was not possible to determine precisely when poles separated from the interzone because during that time the chromosomes may partially obscure fluorescence near the pole. We believe that the microtubule detachment is likely to be complete by the time of nuclear reformation. This period could be recognized by the swelling and rounding of the dark chromatin masses. Examples of this change can be seen in Fig. 3, *D* and *E*, and in Fig. 7, *C* and *D*. The timing of the nuclear transition in the cell shown in Fig. 7 is marked on the graph in Fig. 9. The data points in Fig. 9 show that the movement of interzone halves away from one another continued during and after nuclear reformation. Some of the movement then may be independent of a direct microtubule connection between the spindle poles and interzone.

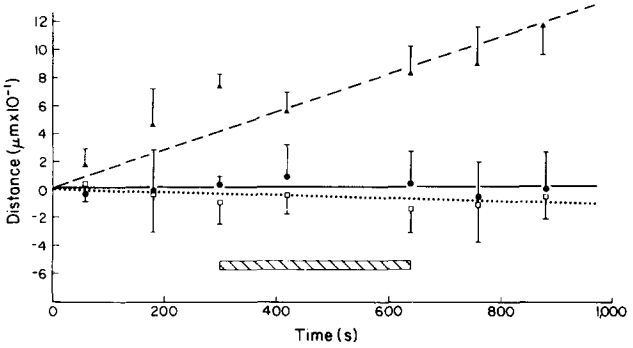

Figure 9. Changes in interzone distances as a function of time. The mean values for changes between points marked on fluorescent interzone microtubules as determined by analysis of the images in Fig. 7 were plotted as a function of time after photobleaching, and fitted with straight lines by linear regression forced through the origin. Changes are shown within the left half-spindle (*squares, dotted line*), within the right half-spindle (*solid circles, solid line*), and between left and right half-spindles (*triangles, dashed line*). The slopes of the lines reflect average rates of movement. The shaded bar marks the time interval over which noticeable chromosome decondensation occurred.

Table II. Movement of Bleach Markers in Late Anaphase

		Final distance μm × 10^{-1}			Average rate μm/min × 10^{-2}		
Cell	Time	Left	Right	Left-right	Left	Right	Left-right
No.	*s*						
1	880	−0.9	1.4	13.0	0.17	0.46	8.7
2	420	−0.4	−4.5	5.0	−0.45	−0.48	6.0
3	880	0.0	−0.4	11.9	0.06	−0.73	8.2
4	420	−1.4	0.0	8.1	−0.20	0.64	12.5
5	760	0.0	0.4	5.6	−0.02	0.05	3.7
6	420	−2.7	0.4	12.6	−0.25	0.31	17.8

Discussion

The results presented here support models of anaphase spindle elongation that include addition of microtubule subunits to the pole-distal ends (plus ends) of the interdigitated microtubules. Also, the results suggest that plus end subunit addition can be accompanied by antiparallel sliding apart of the two interdigitated half-spindles, perhaps driven by forces that are generated within the spindle. The data provide the first direct in vivo evidence for tubulin addition to the plus ends of the interdigitated microtubules. This is also the first direct evidence that antiparallel sliding of interdigitated microtubules can occur in spindles other than the highly organized ones found in some diatoms. Furthermore, striking differences in microtubule turnover in neighboring parts of the spindle show that there are factors controlling microtubule dynamics that are not freely diffusible.

In Vivo Comparison of Native and DTAF-Tubulin

In studies that use a derivatized protein to explore the behavior of its native counterpart, it is necessary to determine how normal the behavior of the derivatized protein is. We have previously compared the polymerization behavior of native and DTAF-tubulin in vitro and found only minor differences (21). We have also compared the cellular distribution of microinjected DTAF-tubulin with that of all microtubules in fixed cells and found them to be essentially indistinguishable (37). Further, the in vivo responses of DTAF-tubulin–containing microtubules to taxol and nocodazole appeared to be the same as those of native microtubules, and the presence of DTAF-tubulin in cellular microtubules did not disrupt microtubule-based movements such as mitosis and interphase particle saltation (35, 37). Here we have compared native and DTAF-tubulin more directly. We found that either native or DTAF-tubulin will effect a partial mitotic rescue when microinjected into taxol-dependent CHO cells (Tax-18) growing in taxol-free medium. Cabral's cytological studies of Tax-18 indicate that the mitotic spindle assembly mechanism is impaired and that it is probably the enhancement of microtubule polymerization by taxol that promotes successful mitotic division (6). A reasonable interpretation of the microinjection-rescue results described here is that the increase in the concentration of intracellular tubulin which results from microinjection provides an enhancement of microtubule polymerization similar in effect to that provided by taxol, and thereby promotes successful mitotic division. Identification of the genetic lesion in this mutant and a characterization of the aberrant gene product will be necessary

for a rigorous understanding of the mechanism involved in the tubulin-mediated rescue. Regardless of the precise mechanism, however, mitotic rescue by microinjection provides a method for direct comparison of the functional behaviors of native and DTAF-tubulin in vivo. The two are very similar.

In a second comparison, we have found that either native or DTAF-tubulin complexed with colchicine will cause rapid depolymerization of spindle microtubules when microinjected into mitotic cells. The effects of the two different complexes are similar. This suggests that native and DTAF-tubulin are similar in terms of colchicine-induced spindle depolymerization. It is widely believed that tubulin–colchicine complex exerts its effect by incorporating into the microtubule lattice (23, 40). Our result therefore implies that DTAF-tubulin incorporates into the tubulin lattice of microtubules by a normal pathway.

Results from the colchicine–tubulin experiment and the mutant rescue experiment described above increase our confidence in DTAF-tubulin as a reporter of endogenous tubulin activities in living cells. They have also, however, introduced a note of caution. In both experiments, DTAF-tubulin seemed to be slightly less active than native tubulin, so when it is used to trace tubulin processes in cells, it may result in underestimates of the rates of those processes.

Of more general significance is the result that tubulin–colchicine complex is more effective at spindle depolymerization than is free colchicine. This supports Taylor's hypothesis that the binding of colchicine to tubulin dimers is a rate-limiting step in the mechanism of colchicine-induced microtubule depolymerization in vivo (41).

Tubulin Dynamics in General

The evidence that prophase and metaphase microtubules turn over at approximately 20 times the rate of interphase microtubules raises the question of what controls the difference in behavior (37). One possibility is that the cytoplasm of an interphase cell changes during the transition to prophase, thus causing rapid microtubule turnover. However, the experiments reported here suggest that polar microtubules in the chromosomal half-spindles turn over rapidly while the neighboring interdigitated microtubules do not. This argues against the possibility that rates of turnover are controlled simply by "cytoplasmic state" or factors in the cytoplasm that are freely diffusible. It is likely that the rate of tubulin turnover in a particular microtubule is partly determined by its own composition or by its association with nondiffusible components of cytoplasm (13, 32, 38). The timing of the change we have seen from apparently homogeneous microtubule dynamics in metaphase and early anaphase to heterogeneous dynamics in late anaphase may have some bearing on this question. It is during the period from early to late anaphase that the plus ends of the interdigitated microtubules begin to exhibit interaction with one another (30). It is possible that the molecular details of this interaction prevent the interdigitated microtubules from participating in the rapid turnover phenomenon, and instead promote tubulin addition to their plus-ends.

Late Anaphase–Telophase Interzone Elongation in PtK$_1$ Cells

In studying the patterns of incorporation of injected DTAF-tubulin and the patterns of tubulin FRAP, we have obtained evidence that tubulin adds to the plus ends of elongating interdigitated microtubules during late anaphase-telophase. When a late anaphase cell is microinjected with DTAF-tubulin, fluorescence incorporation is heterogeneous along the spindle axis. A rapid appearance of fluorescence in the chromosomal half-spindle is followed by a slow increase in fluorescence at the equator of the interzone. When the interzone of a fluorescent anaphase spindle is photobleached, there is a noticeable heterogeneity in the pattern of fluorescence redistribution. There is a fast redistribution, due to the diffusion of soluble DTAF-tubulin back into the bleached region, followed by the appearance of fluorescent streaks that run parallel to the spindle axis on either side of the equator. With time, the pattern of fluorescence changes to a bright area at the equator flanked by two dark areas.

These two patterns of DTAF–tubulin addition correlate with the probable patterns of distribution of the plus ends of interdigitated microtubules during late anaphase and telophase (9, 28, 30). A reasonable model that accounts for the two patterns and the transition between them follows. (*a*) In late anaphase, tubulin adds to the plus ends of the elongating interdigitated microtubules. Since they are of diverse lengths and collected into interzone fibers at that time, added fluorescent tubulin appears as longitudinal streaks. (*b*) As late anaphase proceeds, the two sets of interdigitated microtubules slide in opposite directions. The sliding coincides with or causes a more uniform distribution of lengths. The result is that the fluorescent segments at the ends of the interdigitated microtubules come into register at the equator forming a bright band there at telophase.

Note, however, that the assignment of a site of tubulin addition to the plus ends of interdigitated microtubules is really through inference. The largest increases in fluorescence after photobleaching correlate with the greatest concentrations of interdigitated plus ends. Control experiments described here and previously suggest that high concentrations of fluorescence in a microinjected cell are a result of the incorporation of DTAF-tubulin into microtubules and that photobleaching does not alter the in vivo behavior of DTAF-tubulin (37). Therefore the fluorescence patterns in the interzone suggest that tubulin adds to the plus ends of interdigitated microtubules. However, other mechanisms of local tubulin sequestration may be possible. A more rigorous analysis will require a study of interzone FRAP by electron microscopy. This could be accomplished by using an antibody that binds fluorescent tubulin but not bleached fluorescent tubulin (11, 36) with electron microscope immunocytochemistry.

The model of late anaphase–telophase spindle behavior described above calls for the antiparallel sliding of interdigitated microtubules as well as for the addition of tubulin to their plus ends. We have tested the possibility of microtubule sliding by marking fluorescent interzone microtubules with a series of lines bleached perpendicular to the pole-to-pole axis, and then measuring movements between the bleached marks. When these measurements are collected into three groups, representing changes in distances within the left half-spindle, within the right half-spindle, and between the two half-spindles, an analysis of different models for spindle elongation is possible. The predictions of three current models are diagrammed in Fig. 10. If interdigitated microtubules elongate by polymerization only at their plus ends and undergo antiparallel sliding (24, 27), then the mean changes in spacings within the left and right half-spindles should be

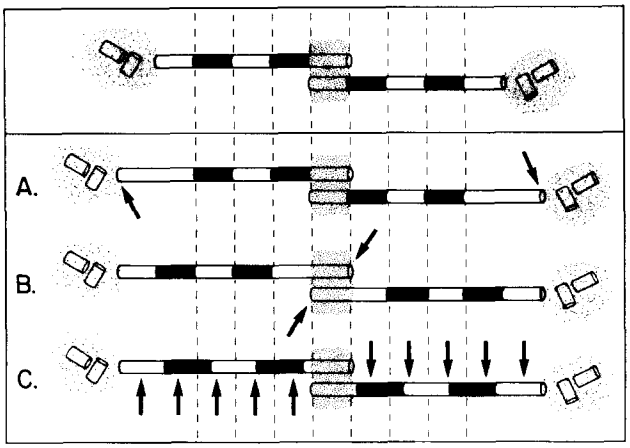

Figure 10. Models of spindle elongation. Shifts in grating bleach patterns predicted by the different possibilities for sites of tubulin addition to interdigitated microtubules. Fine stipling represents "centrosomal material" around the centrioles, and coarse stipling shows "midbody material" in the zone of interdigitation. The upper panel represents two late-anaphase microtubules extending from the spindle poles to interdigitate at the equator. The black and white bands in the microtubules represent the bleached and unbleached areas that are produced in a grating photobleach experiment. Arrows in *A–C* mark possible sites of tubulin addition during spindle elongation. Minus end addition (*A*) would not lead to any changes in the spacing of the grating pattern. Plus end addition and antiparallel sliding (*B*) would preserve the spacings of the grating pattern within each microtubule but would also shift the two away from one another, increasing the width of the bright zone at the equator. Addition at multiple sites along the microtubule walls (*C*) would lead to the movement of all points in the grating pattern away from one another.

zero while the mean change in spacings between half-spindles should be greater than zero. If interdigitated microtubules elongate by polymerization only at their minus ends (34) then all three mean changes should be zero. Finally, if interdigitated microtubules elongate by insertion of subunits along their walls (17) then all three mean changes should be greater than zero.

The data seen in Figs. 8 and 9 and Table II clearly support the model involving polymerization at plus ends and antiparallel sliding. The mean changes are near zero within the half-spindles while the mean change between half-spindles is significantly greater than zero. The results exclude the possibility of extensive subunit addition all along the walls of interdigitated microtubules. They do not, however, exclude the possibility of subunit addition at the minus as well as at the plus ends, since the effects of minus end addition would be silent in this test. In principle, one should be able to observe polymerization at the minus ends of interdigitated microtubules with fluorescent tubulin, but in our experiments the fluorescence of the pole region represents astral, polar, and kinetochore as well as interdigitated microtubules. When photobleached during late anaphase-telophase, the pole region shows a rapid redistribution of DTAF-tubulin (31), similar in rate to that seen in metaphase spindles (35–37). It is likely that this highly dynamic behavior is due to the rapid turnover of polar microtubules, but the possibility of addition to the minus ends of interdigitated microtubules should still be considered. A detailed examination of FRAP by electron microscopy could resolve this question.

A less direct way of addressing the question of the participation of minus end addition would be to compare the rate of spindle elongation with the rate of antiparallel sliding of half-spindles. If the rates are equal, then elongation must be through sliding and plus end polymerization. If not, then polymerization must also be occurring at the minus ends. It has not been possible to measure the rate of spindle elongation accurately during grating FRAP because the spindles enter telophase during observation. The poles appear to detach from the interzone at this time and no longer serve as good markers for the minus ends of the interdigitated microtubules. We were unsuccessful in attempts to execute successful grating FRAP experiments earlier in anaphase. During the most rapid period of spindle elongation the interzone is not long enough to accommodate a full grating pattern and the interzone fibers are not yet well organized. When it is long enough and sufficiently organized to permit measurement of the movements of interdigitated microtubules, most of spindle elongation is over. Brinkley and Cartwright have made careful measurements of the rate of pole separation during PtK_1 anaphase and reported rates of up to 2 μm/min (3). We have confirmed that these rates occur in our particular cell line. During late stages of anaphase B and telophase, we have recorded antiparallel sliding rates of up to 0.18 μm/min.

It should be emphasized that our investigation of the mechanism of spindle elongation in PtK_1 rests mainly on experimentation done in late anaphase and telophase when most of the elongation was already complete. It is possible that the microtubule behaviors we have observed are not connected with earlier stages of elongation, perhaps being part of a separate movement (3). Our opinion is that the plus end polymerization and slow sliding seen in these experiments were the final stages of the more extensive spindle elongation that occurred earlier. We infer that the early and late interzone elongations occur by the same mechanism.

Force Production for Anaphase B

One important question about mitosis is how the force for spindle elongation is produced. Aist and Berns have obtained evidence that in *Fusarium* there is a force generated outside the spindle that acts on the poles, and pulls the interdigitated half-spindles away from one another (1). Kronebusch and Borisy have suggested that the astral microtubules, which extend from the poles away from the spindle could produce such a pulling force in PtK_1 cells (19). On the other hand, observations by Berkeley (2) and Carlson (8) suggest that in *Amoeba* and grasshopper neuroblasts, elongation is due to a forceful extension of the interpolar spindle. Leslie and Pickett-Heaps have convincingly demonstrated that the spindle elongation force in *Hantzschia* is generated in the interzone (20). Work by Cande and McDonald (7) and more recently by Masuda and Cande (25) in vitro on spindles isolated from diatoms show not only that force is generated in the interzone but also that the resultant antiparallel sliding is enhanced by the addition of tubulin to the plus ends of the interdigitated microtubules.

Our antitubulin immunofluorescence and DTAF–tubulin images suggest that late in anaphase the poles free themselves from the interdigitated microtubules. The microtubules might be released by the centrosome or they might be severed near it. Some of the antiparallel sliding that we have measured appears to occur after the poles are detached from

the interzone microtubules. This suggests that a force-producing mechanism for antiparallel microtubule sliding in PtK_1 spindles resides within the spindle and, more specifically, within the interzone.

In summary, we have studied late anaphase–telophase spindle behavior in living mammalian cells. Our results suggest that (*a*) the dynamic behavior of mitotic microtubules is determined in part by their own composition or by association with nondiffusible components of the cytoplasm; (*b*) interdigitated microtubules add tubulin to their plus ends; (*c*) interdigitated microtubules can undergo antiparallel sliding; and (*d*) a force for this sliding may be generated within the interzone.

We thank Derek Stemple for his invaluable help in developing the analysis procedures and Susan Strome for stimulating discussions and critical reading of the manuscript.

This work was supported by GM33787 from the National Institutes of Health and by RR07013 from the Biomedical Research Support Grant Program, Division of Research Resources, National Institutes of Health.

Received for publication 18 November 1986, and in revised form 22 April 1987.

References

1. Aist, J. R., and M. W. Berns. 1981. Mechanics of chromosome separation during mitosis in *Fusarium (Fungi imperfecti)* new evidence from ultrastructural and laser microbeam experiments. *J. Cell Biol.* 91:446–458.
2. Berkeley, E. 1948. Spindle development and behavior in the giant amoeba. *Biol. Bull.* 94:169–175.
3. Brinkley, B. R., and J. Cartwright, Jr. 1971. Ultrastructural analysis of mitotic spindle elongation in mammalian cells *in vitro*. *J. Cell Biol.* 50:416–431.
4. Cabral, F. 1983. Isolation of Chinese hamster ovary cell mutants requiring the continuous presence of taxol for cell division. *J. Cell Biol.* 97:22–29.
5. Cabral, F., and M. M. Gottesman. 1979. Phosphorylation of the 10-nm filament protein from Chinese hamster ovary cells. *J. Biol. Chem.* 254: 6203–6206.
6. Cabral, F. R., R. C. Brady, and M. J. Schibler. 1986. A mechanism of cellular resistance to drugs that interfere with microtubule assembly. *Ann. N. Y. Acad. Sci.* 466:745–756.
7. Cande, W. Z., and K. L. McDonald. 1985. *In vitro* reactivation of anaphase spindle elongation using isolated diatom spindles. *Nature (Lond.)* 316: 168–170.
8. Carlson, J. G. 1952. Microdissection studies of the dividing neuroblast of the grasshopper. *Chortophaga viridifasciata* (DeGeer). *Chromosoma (Berl.)*. 5:199–220.
9. Euteneuer, U., and J. R. McIntosh. 1980. Polarity of midbody and phragmoplast microtubules. *J. Cell Biol.* 87:509–515.
10. Garland, D. L. 1978. Kinetics and mechanism of colchicine binding to tubulin: evidence for ligand-induced conformational change. *Biochemistry*. 17:4266–4272.
11. Gorbsky, G. J., P. J. Sammak, and G.G. Borisy. 1987. Chromosomes move poleward in anaphase along stationary microtubules that coordinately disassemble at their kinetochore ends. *J. Cell Biol.* 104:9–18.
12. Graessman, A., M. Graessman, and C. Mueller. 1980. Microinjection of early SV40 DNA fragments and T antigen. *Methods Enzymol.* 65:816–825.
13. Gunderson, G. G., S. Khawaja, and J. C. Bulinsky. 1987. Post-polymerization detyrosination of alpha-tubulin: a mechanism for subcellular differentiation of microtubules. *J. Cell Biol.* In press.
14. Hamel, E., and C. M. Lin. 1981. Glutamate-induced polymerization of tubulin: characteristics of the reaction and application to large-scale purification of tubulin. *Arch. Biochem. Biophys.* 209:29–40.
15. Heath, B. 1980. Variant mitoses in lower eukaryotes: indicators of the evolution of mitosis? *Int. Rev. Cytol.* 64:1–80.
16. Hiller, G., and K. Weber. 1978. Radioimmunoassay for tubulin: a quantitative comparison of the tubulin content of different established tissue culture cells and tissues. *Cell*. 14:795–804.
17. Inoue, S., and H. Sato. 1967. Cell motility by labile association of molecules: the nature of mitotic spindle fibers and their role in chromosome movement. *J. Gen. Physiol.* 50:259–292.
18. Keith, C. H., J. R. Feramisco, and M. Shelanski. 1981. Direct visualization of fluorescein-labeled microtubules *in vitro* and in microinjected fibroblasts. *J. Cell Biol.* 88:234–240.
19. Kronebusch, P.J., and G. G. Borisy. 1982. Mechanics of anaphase B movement. *In* Biological Functions of Microtubules and Related Structures. H. Sakai, H. Mohri, and G. G. Borisy, editors. Academic Press, Inc., New York. 233–245.
20. Leslie, R. J., and J. D. Pickett-Heaps. 1983. Ultraviolet microbeam irradiations of mitotic diatoms: investigation of spindle elongation. *J. Cell Biol.* 96:548–561.
21. Leslie, R. J., W. M. Saxton, T. Mitchison, B. Neighbors, E. D. Salmon, and J. R. McIntosh. 1984. Assembly properties of fluorescein-labeled tubulin *in vitro* before and after fluorescence photobleaching. *J. Cell Biol.* 99:2146–2156.
22. Manton, I., K. Kowallik, and H. A. von Stosch. 1970. Observations on the fine structure and development of the spindle at mitosis and meiosis in a marine centric diatom *(Lithodesmium undulatum)*. IV. The second meiotic division and conclusion. *J. Cell Sci.* 7:407–443.
23. Margolis, R. L., and L. Wilson. 1977. Addition of colchicine-tubulin complex to microtubule ends: the mechanism of substoichiometric colchicine poisoning. *Proc. Natl. Acad. Sci. USA*. 74:3466–3470.
24. Margolis, R. L., L. Wilson, and B. I. Kiefer. 1978. Mitotic mechanism based on intrinsic microtubule behavior. *Nature (Lond.)*. 272:450–452.
25. Masuda, H., and W. Z. Cande. 1987. The role of tubulin polymerization during spindle elongation *in vitro*. *Cell*. In press.
26. McDonald, K. L., M. K. Edwards, and J. R. McIntosh. 1979. Cross-sectional structure of the central mitotic spindle of *Diatoma vulgare*. Evidence for specific interactions between anti-parallel microtubules. *J. Cell Biol.* 83:443–461.
27. McIntosh, J. R. 1985. Spindle structure and mechanisms of chromosome movement. *In* Aneuploidy: Etiology and Mechanisms. V. L. Delarco, P.E. Voytec, and A. Holleander, editors. Plenum Publishing Corp., New York. 197–229.
28. McIntosh, J. R., W. Z. Cande, and J. A. Snyder. 1975. Structure and physiology of the mammalian mitotic spindle. *In* Molecules and Cell Movement. S. Inouye and R. E. Stephens, editors. Raven Press, New York. 31–76.
29. McIntosh, J. R., P. K. Hepler, and D. G. Van Wie. 1969. Model for mitosis. *Nature (Lond.)*. 224:659–663.
30. McIntosh, J. R., U.-P. Roos, B. Neighbors, and K. L. McDonald. 1985. Architecture of the microtubule component of mitotic spindles from *Dictyostelium discoideum*. *J. Cell Sci.* 75:93–129.
31. McIntosh, J. R., W. M. Saxton, D. L. Stemple, R. J. Leslie, and M. J. Welsh. 1986. Dynamics of tubulin and calmodulin in the mammalian mitotic spindle. *Ann. N. Y. Acad. Sci.* 466:566–579.
32. Mitchison, T., L. Evans, E. Schulze, and M. Kirschner. 1986. Sites of microtubule assembly and disassembly in the mitotic spindle. *Cell*. 45: 515–527.
33. Ostergren, G. 1949. *Luzula* and the mechanism of chromosome movements. *Hereditas*. 35:445–468.
34. Pickett-Heaps, J. D., D. H. Tippit, S. A. Cohn, and T. P. Spurck. 1986. Microtubule dynamics in the spindle: theoretical aspects of assembly/disassembly reactions *in vivo*. *J. Theoret. Biol.* 118:153–169.
35. Salmon, E. D., R. J. Leslie, W. M. Saxton, M. L. Karow, and J. R. McIntosh. 1984. Spindle microtubule dynamics in sea urchin embryos. Analysis using fluorescein-labeled tubulin and measurements of fluorescence redistribution after laser photobleaching. *J. Cell Biol.* 99:2165–2174.
36. Saxton, W. M. 1986. Tubulin and microtubule dynamics *in vivo*. Ph.D. thesis, University of Colorado. 181 pp.
37. Saxton, W. M., D. L. Stemple, R. J. Leslie, E. D. Salmon, and J. R. McIntosh. 1984. Tubulin dynamics in cultured mammalian cells. *J. Cell Biol.* 99:2175–2186.
38. Schulze, E., and M. Kirschner. 1986. Microtubule dynamics in interphase cells. *J. Cell Biol.* 102:1020–1031.
39. Soltys, B. J., and G. G. Borisy. 1985. Polymerization of tubulin *in vivo*: direct evidence for assembly onto microtubule ends and from centrosomes. *J. Cell Biol.* 100:1682–1689.
40. Sternlicht, H., and I. Ringel. 1979. Colchicine inhibition of microtubule assembly via copolymer formation. *J. Biol. Chem.* 254:10540–10550.
41. Taylor, E. W. 1965. The mechanism of colchicine inhibition of mitosis. I. Kinetics of inhibition and the binding of H^3-colchicine. *J. Cell Biol.* 25:145–160.
42. Tippit, D. H., C. T. Fields, K. L. O'Donnell, J. D. Pickett-Heaps, and D. J. McLaughlin. 1984. The organization of microtubules during anaphase and telophase spindle elongation in the rust fungus *Puccinia*. *Eur. J. Cell Biol.* 34:34–44.
43. Tippit, D. H., L. Pillus, and J. D. Pickett-Heaps. 1980. Organization of spindle microtubules in *Ochromonas danica*. *J. Cell Biol.* 87:531–545.
44. Tippit, D. H., L. Pillus, and J. D. Pickett-Heaps. 1983. Near-neighbor analysis of spindle microtubules in the alga *Ochromonas*. *Eur. J. Cell Biol.* 30:9–17.
45. Wadsworth, P., and R. D. Sloboda. 1983. Microinjection of fluorescent tubulin into dividing sea urchin cells. *J. Cell Biol.* 97:1249–1254.
46. Weingarten, M. D., M. M. Suter, D. R. Littman, and M. W. Kirschner. 1974. Properties of the depolymerization products of microtubules from mammalian brain. *Biochemistry*. 13:5529–5537.
47. Zavortink, M., M. J. Welsh, and J. R. McIntosh. 1983. The distribution of calmodulin in living mitotic cells. *Exp. Cell Res.* 149:375–385.